Large-Amplitude Forced Vibration Testing for St-Id of Bridges and Foundation Reuse Assessment

FINAL REPORT
January 2020

Submitted by:

Nenad Gucunski, Ph.D.
Professor

Franklin Moon, Ph.D.
Professor

Rutgers, The State University
Richard Weeks Hall of Engineering
500 Bartholomew Road
Piscataway, NJ 08854

External Project Manager
Eddy Germain
Director Bridge Engineering & Infrastructure Mgmt.
New Jersey Department of Transportation
1035 Parkway Avenue
Trenton, NJ 086250

Disclaimer Statement

1. Report No. CAIT-UTC-REG 3	2. Government Accession No.	3. Recipient's Catalog No.
4. Title and Subtitle **Large-Amplitude Forced Vibration Testing for St-Id of Bridges and Foundation Reuse Assessment**		5. Report Date January 2020
		6. Performing Organization Code Rutgers CAIT
7. Author(s) Nenad Gucunski https://orcid.org/0000-0003-3487-2782 Franklin Moon https://orcid.org/0000-0003-3180-9120		8. Performing Organization Report No. CAIT-UTC-REG 3
9. Performing Organization Name and Address Center for Advanced Infrastructure and Transportation Rutgers, The State University of New Jersey 100 Brett Road Piscataway, NJ 08854		10. Work Unit No.
		11. Contract or Grant No. 69A3551847102
12. Sponsoring Agency Name and Address Center for Advanced Infrastructure and Transportation Rutgers, The State University of New Jersey 100 Brett Road, Piscataway, NJ 08854		13. Type of Report and Period Covered Final Report 09/01/2018 – 12/31/2019
		14. Sponsoring Agency Code
15. Supplementary Notes U.S. Department of Transportation/OST-R 1200 New Jersey Avenue, SE Washington, DC 20590-0001		

16. Abstract

This study presents the results of the research on the characterization of unknown bridge foundations by means of dynamic testing for their potential reuse based on the estimation of their ultimate bearing capacity as a limit state. In this project, the applicability of using large-amplitude mobile shakers in tandem with finite element models for sub-structural identification is examined. By exploiting dynamic features of structures, such as dynamic amplification and knowledge of eigenmodes, significantly lower magnitudes of load can be implemented diagnostically as a global nondestructive evaluation (NDE) technique while having notable response levels. The assessment of bridge foundations reuse through the evaluation of the dynamic response of the bridge above the foundation is carried out. This is accomplished by i) examining material properties extracted from dynamic testing of the foundation/soil system to provide empirical estimates of bearing capacity, or ii) evaluating the global dynamic response of the bridge-foundation system and relating it to failure mechanisms. In this report, the known foundation and soil properties problem is presented as a proof of concept. The methodology and preliminary results from field testing and numerical simulations are presented. The unknown foundation and soil properties are addressed in an appendix of the work presented in this report.

17. Key Words Foundation reuse, capacity assessment, nondestructive evaluation, sub-structural identification, dynamic testing		18. Distribution Statement	
19. Security Classification (of this report) Unclassified	20. Security Classification (of this page) Unclassified	21. No. of Pages 35	22. Price

Form DOT F 1700.7 (8-69)

Table of Contents

Contents

List of Figures

List of Tables

PROBLEM DESCRIPTION

In recognition of the safety risks of the aging transportation infrastructure systems under natural and anthropogenic hazards, there has been significant attention paid to the development of reliable safety assessment approaches to support their management, adaption, and reuse. Many of the existing approaches are very complex, time-consuming, expensive, and the level of certainty of obtained results in some cases is insufficient. Structural Identification (St-Id) has evolved over the last several decades to embrace the impressive array of sensing technologies (inclusive of both global sensing and local nondestructive evaluation), highly refined simulation models, and model calibration techniques (both deterministic and probabilistic) now available. St-Id is critical to developing cost-effective and safe approaches to reuse and adapt our existing infrastructure systems, particularly the reuse of bridge foundations.

Foundations of existing bridges can be considered be assets of substantial operational/economic value, which entices their reuse in rehabilitation/reconstruction of bridges. There are numerous studies focusing on the local characterization of foundation integrity parameters, such as concrete strength of footings or resistivity measurements for corrosion potential (Agrawal, Jalinoos, Davis, Hoomaan, & Sanayei, 2018). Moreover, other studies involving dynamic testing were geared towards damage identification in the superstructure. Nevertheless, there is a lack of studies on evaluating the capacity of existing bridge substructure by means of dynamic testing. An exception to this is a study conducted by Olson (2005), which included testing various decommissioned bridges using large-amplitude shakers in a pseudo-destructive manner. It shows that dynamic testing can be used to assess damage in sub/superstructure of bridges. This is done mainly by evaluating loss of vertical stiffness in foundations due to scour or earthquake damage. Furthermore, the evaluation of existing bridge foundations can vary in complexity based on the available information about the substructure. Hence, there is a variety of scenarios that can be encountered with different bridges, including the lack of as-built drawings or geotechnical site exploration/boring logs. The feature of the proposed approach enables a fully nondestructive and rapid assessment of bridges and their components using large mobile shakers as a dynamic excitation source and fast deployable sensor arrays to capture the response. Combined with Structural Identification (St-Id), the proposed evaluations will provide information about the global bridge condition, assess the need for system adaption, and in the case of a superstructure and/or substructure replacement, assess the feasibility of the foundation reuse.

The project aims to overcome the limitations of existing dynamic testing methodologies for structural and foundation systems. While cost-effective, existing methodologies suffer from reliance on low-amplitude, which is unable to overcome intermittent stick-slip mechanisms or to induce appreciable responses within the substructure-foundation system. In the case of foundation reuse assessment, the bearing capacity estimates are far more accurate if the foundation response is moved into a non-linear range. Therefore, to overcome these low-level mechanisms in a controlled manner and improve the reliability of St-Id, the research team will, in addition to analytical and numerical simulation tools, use large-amplitude mobile shakers that are available through the NSF NHERI Program. Such shakers open opportunities for pushing the structural-foundation systems beyond their low-level response to reveal performance characteristics that are more representative of the expected behavior under safety limit states.

APPROACH

In order to assess the potential reuse of the substructure, the ultimate bearing capacity will be the basis of judging the substructure reusability herein. The bearing capacity can be fundamentally defined as the average contact pressure between the load-bearing soil and the bottom surface of the foundation/substructure under a given limit state. From a structural/mechanical point of view, there are primarily three limit states: i) critical state (when a failure mechanism takes place), ii) serviceability (excessive settlements), and iii) extreme events such as earthquakes (liquefaction). For this project, the critical state condition is used to describe the ultimate bearing capacity herein.

There are several physical properties that play a crucial role in the identification of unknown foundations (L. Olson, Jalinoos, & Aouad, 1998) :

1. Foundation Depth – depth to the bottom soffit of footing, pile length, etc.
2. Foundation Type - shallow vs. deep
3. Foundation Geometry - embedded substructure dimensions, pile locations
4. Foundation Materials - steel, timber, concrete, and masonry
5. Foundation Integrity - corroded steel, rotted timber, cracked concrete, etc

In addition to those, the authors believe that soil properties are also a crucial element in identifying unknown foundations. In this research project, items #4 and #5 are excluded from the evaluation as they are deemed secondary in determining the bearing capacity. Furthermore, since this study serves as a proof of concept, the simpler case of shallow foundations is sought after rather than pile foundations. In addition, a relatively rigid structure in a cohesion-less soil was selected for testing to avoid more complicated/indirect phenomena that can affect the response, such as consolidation or volume change. Therefore, the objective of the study is to estimate the bearing capacity under two different scenarios based on available information:

*   Known foundation geometry and soil properties, and
*   Unknown and foundation soil properties.

This was done by utilizing a large-amplitude shaker on the bridge deck and monitoring response near the foundation and matching it with a 3D Finite Element Model (FEM). The condition with known foundation and soil properties is used as a basis for parametric studies through finite element simulations to investigate the condition with unknown foundation or property, details of the modeling, experimental setup, and methods used to evaluate bearing capacity, are presented in the following sections.

METHODOLOGY

Test Site

Gate Creek overpass on McKenzie Hwy in Vida, Lane County, Oregon, was selected in coordination with Oregon DOT, which fits the desired bridge features; bridge with shallow foundations placed in sandy soil. Fig. 1(a) shows the location of the bridge; the solid lines represent the extent of the bridge. The structure consists of an old part and a new part as a result of a bridge widening project done in 1986. Both parts are multi-span reinforced-concrete bridges on spread footings, but the older part is a ribbed deck supported by a portal frame, while the newer part is supported by a single hammerhead pier. Fig. 1(b) displays the underside of the bridge with different superstructures.

Fig. 1. (a) Tested bridge location and (b) old and new parts of the structure with different superstructures.

T-Rex as a Mobile Shaker for Bridge Tests

T-Rex, a large-amplitude mobile shaker from the Natural Hazards Engineering Research Infrastructure (NHERI) experimental facility at the University of Texas at Austin, was employed to shake the bridge. T-Rex (shown in Fig. 2) is capable of generating large dynamic forces in any of three directions (vertical, horizontal in-line, and horizontal cross-line). To change from one shaking direction to another, the operator simply pushes a button in the driver's cab. The shaking system is housed on an off-road, all-wheel-drive vehicle. The theoretical force outputs of T-Rex in the vertical and both horizontal directions are shown in Fig. 3. The maximum force output is about 267 kN in the vertical mode and about 134 kN in each horizontal mode. The maximum force output is limited by the hold-down weight of the T-Rex truck. Shaking at a higher force output can cause the shaker to decouple (jump) from the ground in the vertical mode or to slide on the ground in the horizontal modes. In the lower frequency range, the force output is limited by the stroke of the reaction mass. In the higher frequency range, the force output is limited by the speed of the hydraulic servo valve. The actual force output depends on the ground condition.

The force output can be measured by load cells, but it requires a stiff ground to support the load cell. For most shaker operations, the ground surface varies from soft soil to concrete pavement, so using load cells is not a practical option. The current method uses accelerometers mounted on the reaction mass and base plate of the shaker from which the force output can be calculated. Fig. 4 shows a close-up photograph of the T-Rex shaker. As shown in the figure, airbags are used to isolate the shaker from the truck. The airbags act as a low pass filter and transfer only static force. If one takes a free body of the T-Rex shaker and ignores the hydraulic system, the only external dynamic force is the dynamic ground force which is also the dynamic force output of T-Rex. The dynamic force output, F_d, can be determined as:

$$F_d = m_{RM} * a_{RM} + m_{BP} * a_{BP} \tag{1}$$

where: m_{RM} is the mass of the reaction mass, a_{RM} is the reaction-mass acceleration, m_{BP} is the mass of the base plate, and a_{BP} is the base-plate acceleration.

The T-Rex on-board Pelton controller was modified to provide an external control option. With the external control option, T-Rex can output an arbitrary waveform generated by an analog waveform generator. The amplitude of the force output is promotional to the amplitude of the arbitrary waveform, and the maximum force output is set at 5 V of the arbitrary waveform. Both chirp and stepped sine functions were used to drive T-Rex for tests on the bridge. In the chirp function, the frequency varies linearly from the start frequency to the end frequency at a given time length. In the stepped sine function, the frequency varies from the start frequency to the end frequency in a given number of steps. The stepped function is ideal for steady-state measurements at small amplitude. The chirp function is a better option at larger amplitude to limit the number of loading cycles (Menq et al., 2008; Stokoe, K., Cox, Clayton, & Menq, 2017).

Fig. 2. A photograph of T-Rex.
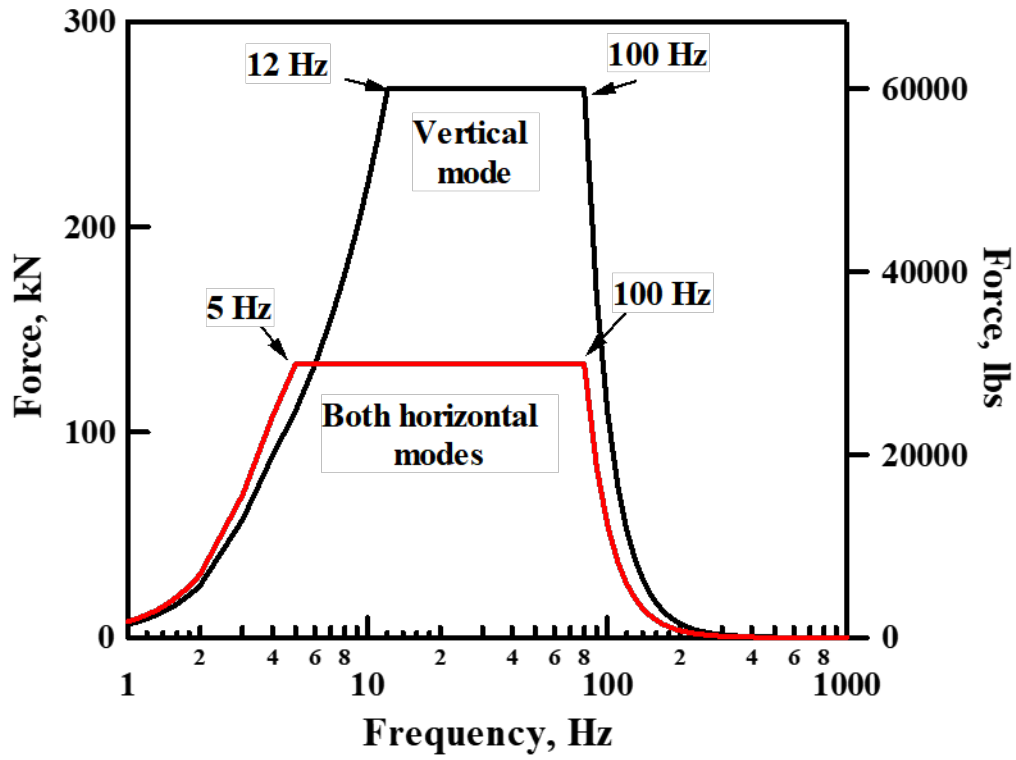
Fig. 3. Theoretical force outputs of T-Rex.
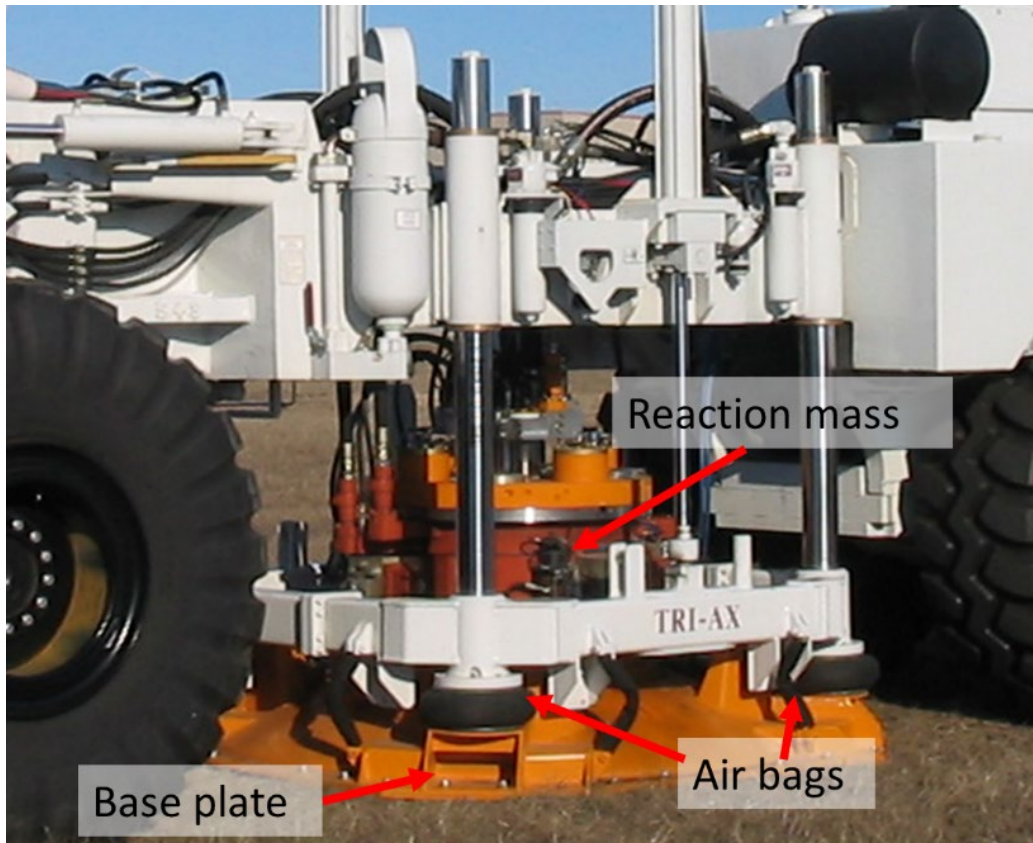
Fig. 4. A close-up photograph of the T-Rex.

Experimental Program

For this project, only the newer part of the bridge was tested. Since the objective of this study was to evaluate the bearing capacity of the underlying footings, only vertical shaking was conducted on the bridge. A local traffic control company was hired to assist with handling traffic and flagging. The testing of the bridge was carried out over two days. On the first day, a chirp loading function at different loading levels was carried out to identify the natural frequencies of the bridge system as a whole. Once the natural frequencies were identified, both the steady-state and ramp-up loading functions were carried out the following day at various frequencies to assess the dynamic amplification of response. A total of 10 geophones (velocity sensors) were deployed to measure the response of the bridge to shaking. The shaking was conducted on three different piers of the new section of the bridge. Therefore the geophones were moved and laid out to capture the response of the excited span and respective pier. In this report, the evaluation of one of the piers/footings is illustrated. Fig. 5 shows a geophone and connecting cable that was used for measuring bridge response while shaking. As for the response for the pier, geophones were attached to the pier 2' above ground with a bolted bracket, as illustrated in Fig. 6. An overall geophone layout for the pier evaluation presented in this report is depicted in Fig. 7.

6

Fig. 5. Typical geophone used for measuring response.

Fig. 6. Geophone attached to the pier to measure response.
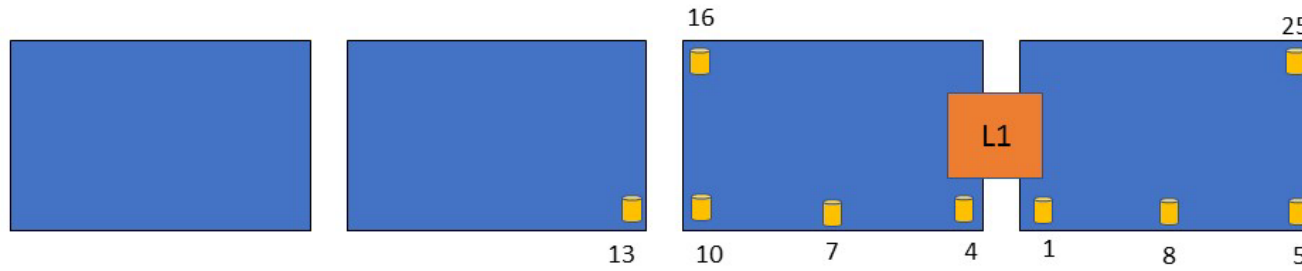
Fig. 7. Overall sensor layout for the tested pier.

Fig. 8 shows T-Rex and the control room on the bridge, ready for shaking. In the control room, the operator is initiating the loading sequence and monitoring the bridge response. Fig. 9 shows the operator monitoring and controlling response in real-time and the waveform generator initiating the T-Rex shaking. Throughout all shaking trials, a maximum response of 1 in/s was set as a vibration level limit. This was to ensure that there is no damage imparted into the bridge within the given frequency range while maximizing the force output as much as possible. Hence, this type of testing is considered a global NDE method. Table 1 presents a summary of T-Rex shake runs conducted above pier 1. The sampling frequency was 1536 Hz, which by far exceeds the Nyquist frequency requirement for the test range.

Fig. 8. T-rex and control room on the bridge ready for shaking.
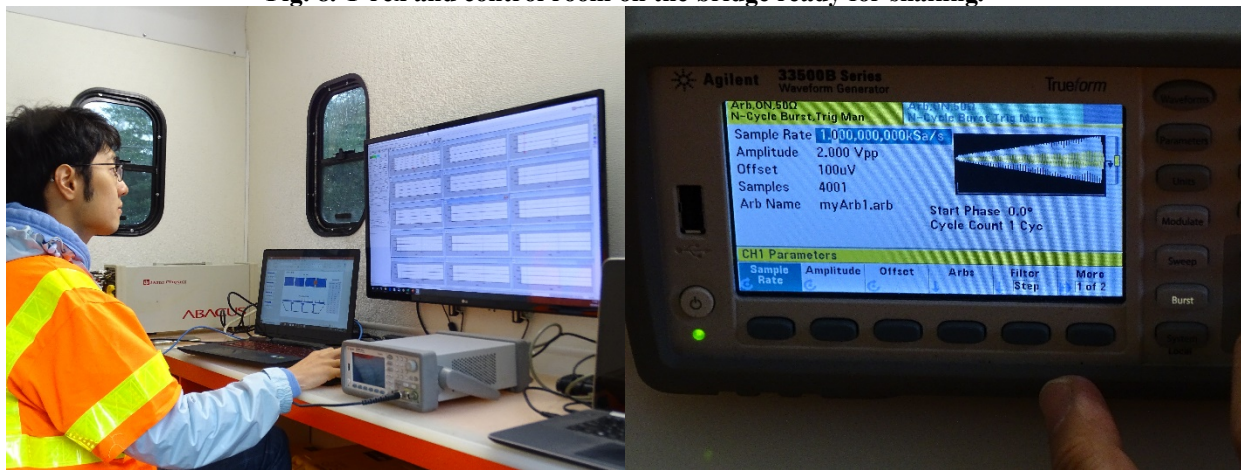
Fig. 9. Left: operator monitoring repose, and right: waveform generator controlling T-rex shaking.

Table 1. Summary of T-Rex Shake Runs in the Experimental Program.

Chirp Mode				
Run	**Start Frequency (Hz)**	**End Frequency (Hz)**	**Drive Voltage (V)**	**Time Length (sec)**
2	80	10	0.2	16
3	15	3	0.2	32
4	80	10	0.4	16
5	15	3	0.4	32
6	80	10	0.8	16
7	15	3	0.8	32
8	80	10	1.5	16
9	15	3	1.5	32
10	80	10	3	16
11	15	3	2.5	32
Steady-State Mode				
Run	**Start Frequency (Hz)**	**End Frequency (Hz)**	**Drive Voltage (V)**	**Time Length (sec)**
3	35	35	2	1.2
4	34	34	2	1.2
5	33	33	2	1.2
6	32	32	2	1.2
7	31	31	2	1.2
8	30	30	2	1.2
9	29	29	2	1.2
10	28	28	2	1.2
11	27	27	2	1.2
12	26	26	2	1.2
13	25	25	2	1.2
14	24	24	2	1.2
15	23	23	2	1.2
16	22	22	2	1.2
17	21	21	2	1.2
18	20	20	2	1.2
19	15	15	2	1.2

Soil Characterization

There were no boring logs/site exploration reports provided from ODOT for the bridge. However, there were results from two test bores (done at the bridge abutments), reporting a Standard Penetration Test (SPT) value of 40 and classifying the soil as very dense sand, with gravel and cobbles, which can also be observed from Fig. 1(b). While this information provides some insight about expected soil mechanical properties, it was just used as a qualitative measure and to estimate the soil density. Instead, a Spectral Analysis of Surface Waves (SASW) was conducted at the bridge site to estimate the soil shear wave velocity (V_s) profile, which is correlated to the response and mechanical properties. From the knowledge of shear wave velocity, the shear modulus (G) can be determined by:

$$G = \rho \, (V_s)^2.$$

(2)

where (ρ) is the mass density of the soil.

In the SASW method, the stiffness of a layered medium is determined through the measurement of the velocity of Rayleigh (surface) waves. In this test, two or more sensors (geophones) were placed on the ground, and a sledgehammer was used to generate a wave on the surface by striking the ground and recording the response at various spacing. Shorter receiver spacing is used to examine shallower layers, while longer spacing is used for deeper layers. The test is performed in two directions to cover the effects of dipping layers and internal phase shifts due to receivers and instrumentation (Nazarian et al., 1983). The source and receiver signals are recorded by a signal analyzer. The cross-power spectrum of signal sat two receiver positions is used to determine the Rayleigh wave velocity with the knowledge of the time or phase delay between receivers as a function of frequency as:

$$t(f) = \phi_{XY}(f) / 360° * f \qquad (2)$$
$$V_r(f) = D.t(f) \qquad (3)$$
$$\lambda r(f) = V_r(f) / f \qquad (4)$$

where $t(f)$ is the time delay as a function of frequency between two receivers, ϕ_{XY} is the phase shift obtained from the cross power spectrum, f is frequency, $V_r(f)$ is Rayleigh wave velocity, D is receiver spacing, and $\lambda r(f)$ is the wavelength as a function of frequency.

The plot of Rayleigh wave velocity vs. wavelength is referred to as the dispersion curve, which is used, in turn, in the inversion process (Gucunski & Woods, 1992). The shear-wave velocity profile is determined by fitting the experimental results (Rayleigh-wave velocity) into a theoretical model of the profile until convergence (best fit) is achieved, which is a numerically intensive procedure. Alternatively, an approximation of shear wave velocity from the Rayleigh wave velocity can be done in uniform soils with regular stratification (velocity increases with depth), which was done in the current research. The approximation is that V_r is 10% lower than the shear wave velocity. Fig. 10 shows the SASW test conducted at the bridge site, and Table 1 provides a summary of SASW runs carried out at the site (locations are in reference to sensor 2 location).

Fig. 10. Left: setting up geophones and adjusting spacing, right: generating acoustic surface wave.

Table 2. Summary of SASW Runs Carried out to Determine Shear Wave Velocity.

Run	Direction	Sensor 1 (ft)	Sensor 2 (ft)	Sensor 3 (ft)	Source Location (ft)
2	F	-1	0	2	-2
3	R	-2	0	1	2
14	F	-2	0	4	-4
15	R	-4	0	2	4
16	R	-4	0	2	4
6	F	-3	0	6	-6
4	R	-6	0	3	6
5	R	-6	0	3	6
7	F	-4	0	8	-8
8	R	-8	0	4	8
10	F	-10	0	20	-20
9	R	-20	0	10	20
11	F	-15	0	30	-30
12	F	-15	0	30	-30
13	R	-30	0	15	30

Numerical Simulation

COMSOL Multiphysics software was used in this study to produce 3D FEM simulations of one of the tested bridge piers, the supported span, and surrounding soil volume. The model solves for the displacement fields as an output in a fully dynamic manner. The studies conducted in the simulations were time-dependent studies to match the response from measurements of the steady-state loading and compare them with the results. The dimensions of the model closely match those of the actual bridge, and all inputs for the model were parametrized, allowing for any combination of sweeps as deemed necessary. Solid elements were used in the model, and linear elastic material properties were assigned since the response was in the elastic range due to the controlled vibration levels. Fig. 11 shows an isometric overview of the 3D model developed in the current study, while Fig. 12 shows the bridge sections illustrating the embedded footing. The block points on the figures are the observation points (either for loading or response measurements).
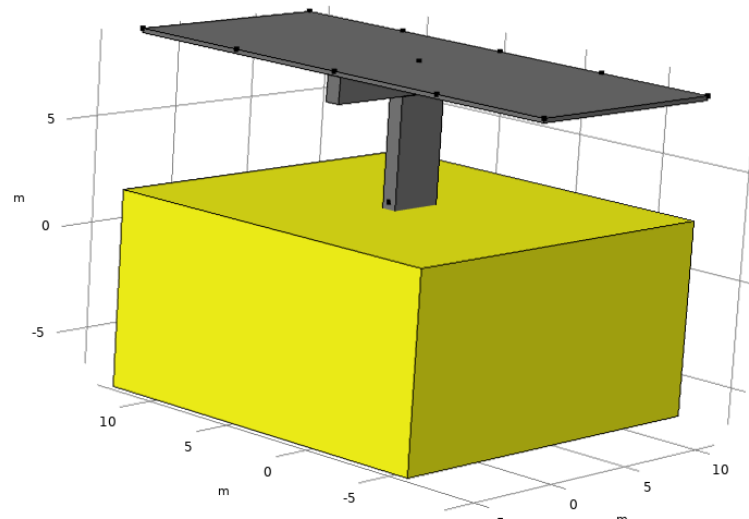
Fig. 11. Bridge overview in 3D model.
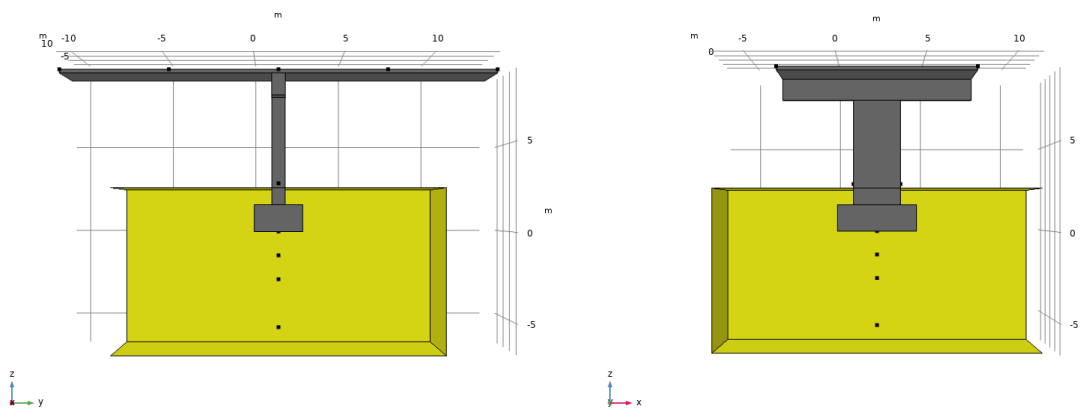
Fig. 12. Profile view indicating the embedded footing.

Table 3 provides a summary of the parameters defined in the study. The mass density of soil was selected to be about 1900 kg/m³. The shear wave velocity value reported in the table is close to the

actual value, as discussed later in the report. It can be observed that the errors in the density used are far less consequential on the shear modulus, and thus the response, compared to the errors in estimating the shear wave velocity since the velocity is a squared quantity. Low-reflecting boundaries were assigned to the side edges of the soil volume to cause the absorption of propagating elastic waves. The bottom edge of the soil was assigned a fixed condition, which represents the bedrock, while the top surface was a free edge (can exhibit displacement). As for the deck, the N-S edges (in the longitudinal directions) were assigned conditions representing a simply-supported span. The soil was assigned a Poisson's ratio of 0.33. For the concrete deck, a modulus of elasticity, density, and Poisson's ratio of 25 GPa, 2,300 kg/m^3, and 0.2 were assigned, respectively. The loading was imposed above the center of the pier, which can be viewed in Fig. 11. To represent the mass of T-Rex, a lumped mass was added to the loading point as well. In addition, gravity loads (self-weight) were included in the study. Fig. 13 shows the intensity of gravity loads. T-Rex weighs 64,000 lbs (~29 tons).

Table 3. Summary of Parameters Included in the Numerical Simulation of Tested Bridge

Label	Expression	Value	Description
P_w	9 [ft]	2.7432 m	Pier width
P_h	20 [ft]	6.096 m	Pier height
P_l	2.5[ft]	0.762 m	Pier length
F_w	9 [ft]	2.7432 m	Footing width
F_h	5 [ft]	1.524 m	Footing thickness
F_l	15[ft]	4.572 m	Footing length
P_{cw}	36[ft]	10.973 m	Pier cap width
P_{ch}	4[ft]	1.2192 m	Pier cap thickness
P_{cl}	2.5 [ft]	0.762 m	Pier cap length
D_w	36[ft]	10.973 m	Deck width
D_h	8 [in]	0.2032 m	Deck thickness
D_l	80[ft]	24.384 m	Deck length
$Soil_B$	60 [ft]	18.288 m	Soil width
$Soil_L$	60 [ft]	18.288 m	Soil length
$Soil_D$	30[ft]	9.144 m	Soil height
D_f	8[ft]	2.4384 m	Footing Depth
V_s	400 [m/s]	400 m/s	Shear Wave velocity
rho	120 [lb/ft^3]	1922.2 kg/m³	Soil Density
G_{max}	rho*(V_s^2)	1.73E8 Pa	Shear Modulus
n_{load}	1	1	Load magnitude modifier
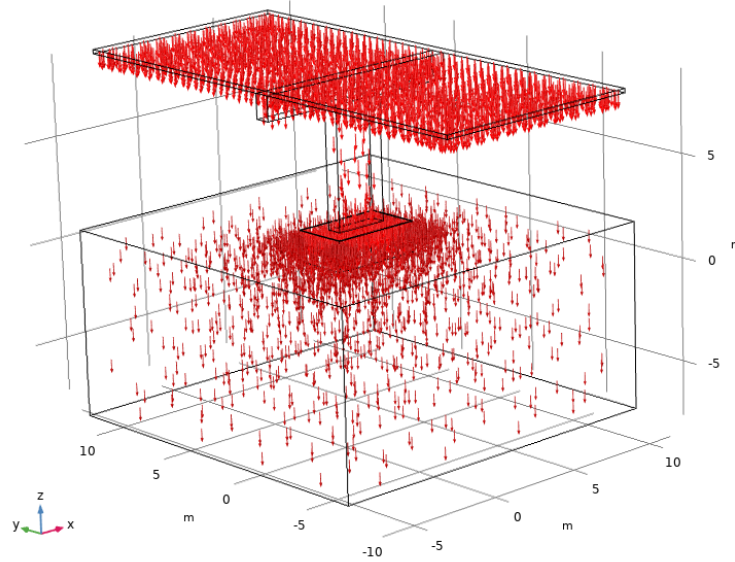
Fig. 13. Intensity of gravity loads in the FEM model.

Rayleigh damping was used to describe the damping characteristics of the bridge superstructure. Rayleigh damping is defined as viscous damping, and is proportional to a linear combination of the mass and stiffness. It is expressed in terms of mass and stiffness as:

$$\xi = \alpha_{dkM}m + \beta_{dk}k, \tag{5}$$

where α_{dkM} is the mass damping parameter, and β_{dk} is the stiffness damping parameter. A value of $\beta_{dk} = 0.001$ was selected to represent the structural damping. $\alpha_{dk} = 0$ was set in the study since inertial effects are low in low-frequency ranges, and the behavior is more stiffness-controlled. In addition, β_{dk} was kept constant to maintain the compatibility and modeling simplicity, although multiple Rayleigh damping ratios at multiple frequencies can lead to more accurate results in the frequency domain. Free tetrahedral elements with adaptive sizing were used to mesh the entire domain. The time-domain studies included a time-step of 0.001 s, with a study span from 0-1.4 s.

FINDINGS

Soil Profile

The SASW test results were analyzed to produce a representative shear wave velocity of the site. Fig. 14 shows sample phase shift between two receivers from the cross-power spectrum of two tests. The receiver spacing is indicated in the legend of each figure. This was done for the tests indicated in Table 2. Results from all tests were then used to produce an overall shear wave velocity profile, which is shown in Fig. 15. It can be observed that the determined range of velocities is in agreement with typical values for dense sand. The higher velocities at deeper portions of the profile are indicative of higher confining pressures and the presence of gravel/cobbles, which was evident in Fig. 1(a) and which validates the profile. Based on the plot in Fig. 15, the shear wave velocity in the zone around the footing was approximated as 400 m/s. This is the reference value for estimation of mechanical properties and matching of the measured response with the one from numerical simulations.
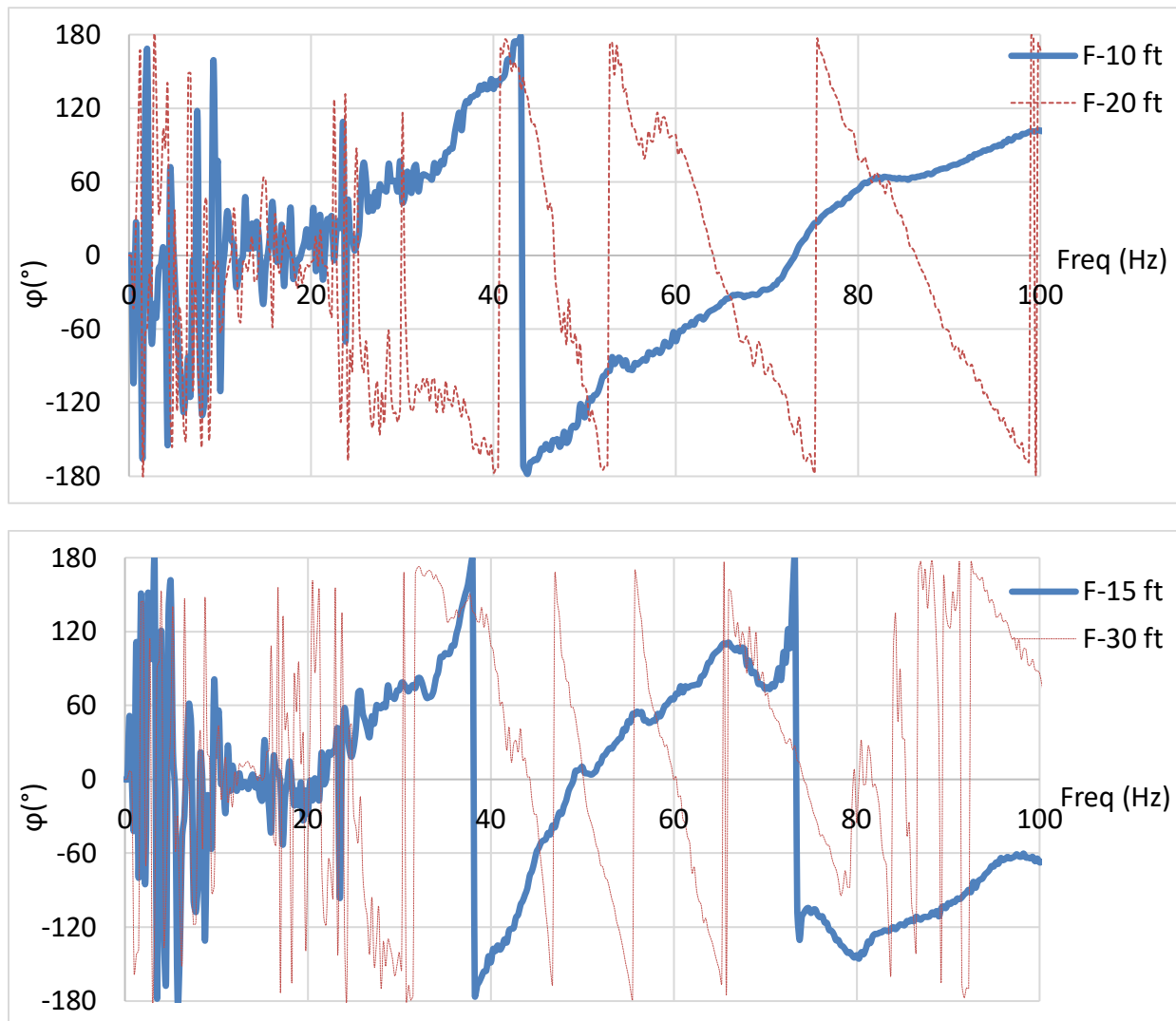
Fig. 14. Phase shift diagrams of two trials with indicated spacing, forward measurement.
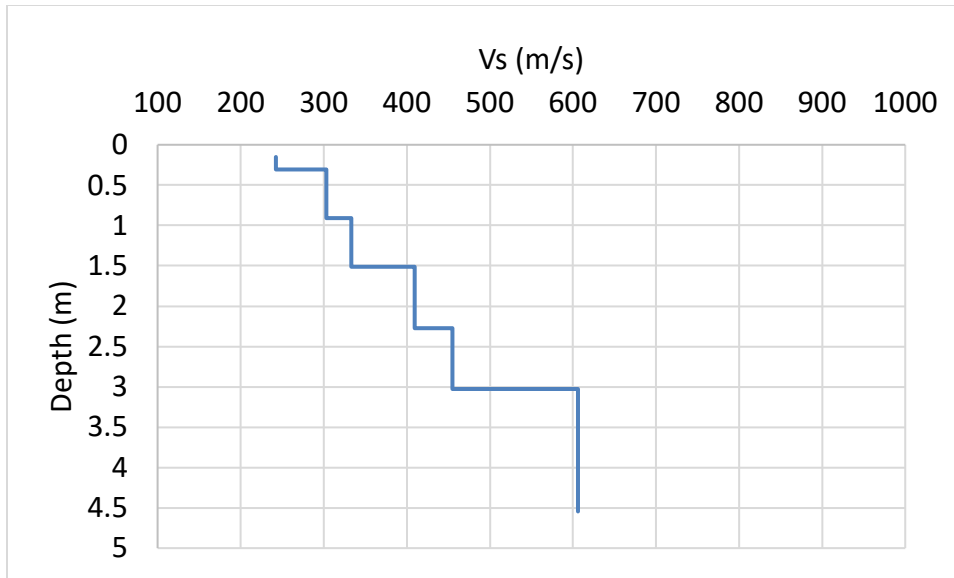
Fig. 15. Experimental shear wave velocity profile of soil at the tested bridge.

Bridge Response

Various bridge response results were obtained from the geophone records. The results include time histories, transfer functions, and phase angles at various locations. The T-Rex loading and the bridge response results are presented in this section. T-Rex was placed above the centerline of the piers in all tests to eliminate potential effects of loading eccentricity. Fig. 16 shows T-Rex with the base plate lowered right above the center of one of the tested piers.

The first set of shakes were done with a linear chirp loading function, in which the frequency was changing at a constant rate over a span of 16 seconds in a frequency range of 10-80 Hz. This was done to identify the natural frequencies of the bridge. Fig. 17 shows the response of a geophone mounted on a pier near the footing and on deck (#19 and #6, respectively in Fig. 7) to chirp loading under various load levels.

Fig. 16. T-rex loading one of the tested piers of the bridge.
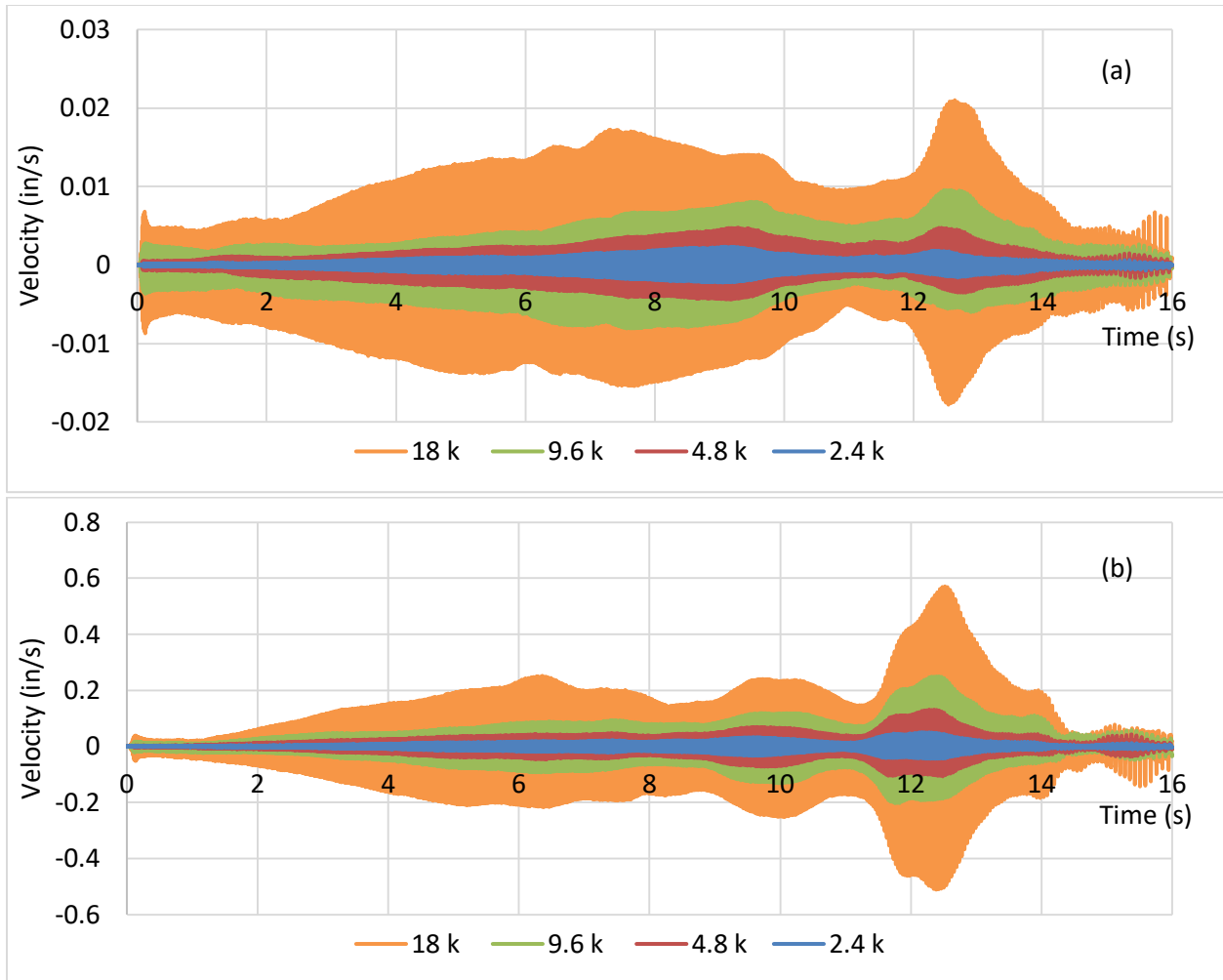
Fig. 17. Footing response to chirp loading under various load levels at (a) the footing and (b) the deck level.

The response of the deck is orders-of-magnitude higher than that of the footing at lower load levels, but this gap diminishes as the load increases. This is illustrated in Fig. 18, which shows the response for both locations when the load was increased to 36 k [160 kN], which was the highest load applied in the chirp loading. The maximum response at the deck level was ~1.2 in/s [30.48 mm/s], compared to 0.3 in/sec [7.62 mm/s] at the footing level. This means that there is a better load transfer mechanism and engagement of the entire structure, as opposed to lower magnitude loads. This is a significant advantage of using large-amplitude mobile shakers for exploring dynamic features of soil/structure systems as opposed to other low-level load conventional methods, such as traveling vehicles. In order to determine the natural frequencies, the power spectra of the time histories were obtained through Fast Fourier Transforms (FFTs). The records of the highest load magnitude were used in this step, which is presented in Fig. 18. Additional sweeps, as indicated in Table 2 were carried out in order to identify resonances in lower frequency ranges (3-15 Hz), as shown in Fig. 19. Fig. 20 shows the power spectra at (a) the deck and (b) footing for the 80-10 Hz range, while Fig. 21 shows the same for the 15-3 Hz range.

18
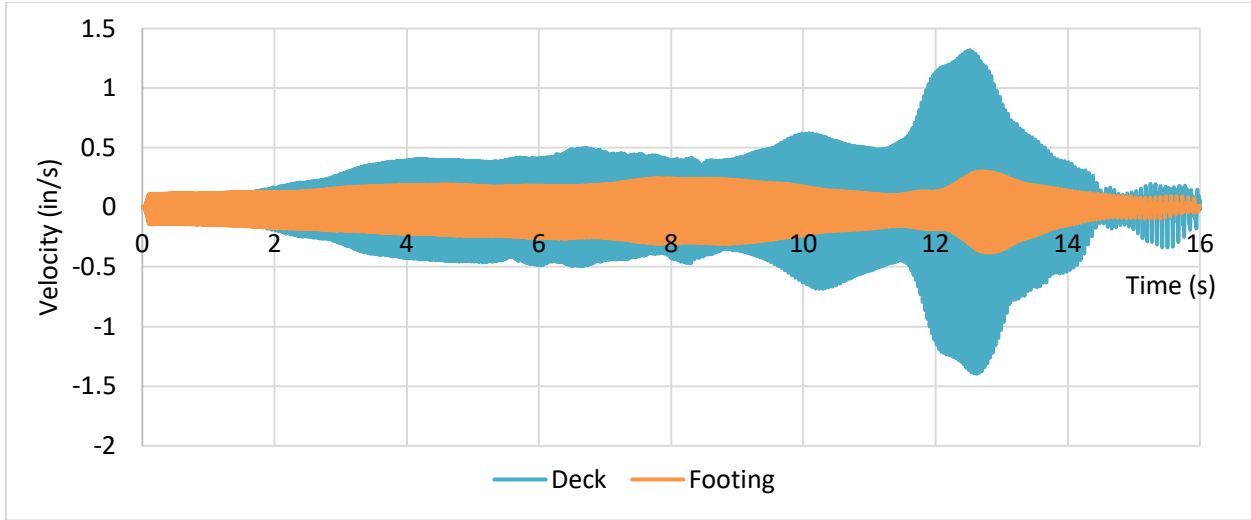
Fig. 18. Response of footing and deck to a 36 k chirp loading function (80-10 Hz)
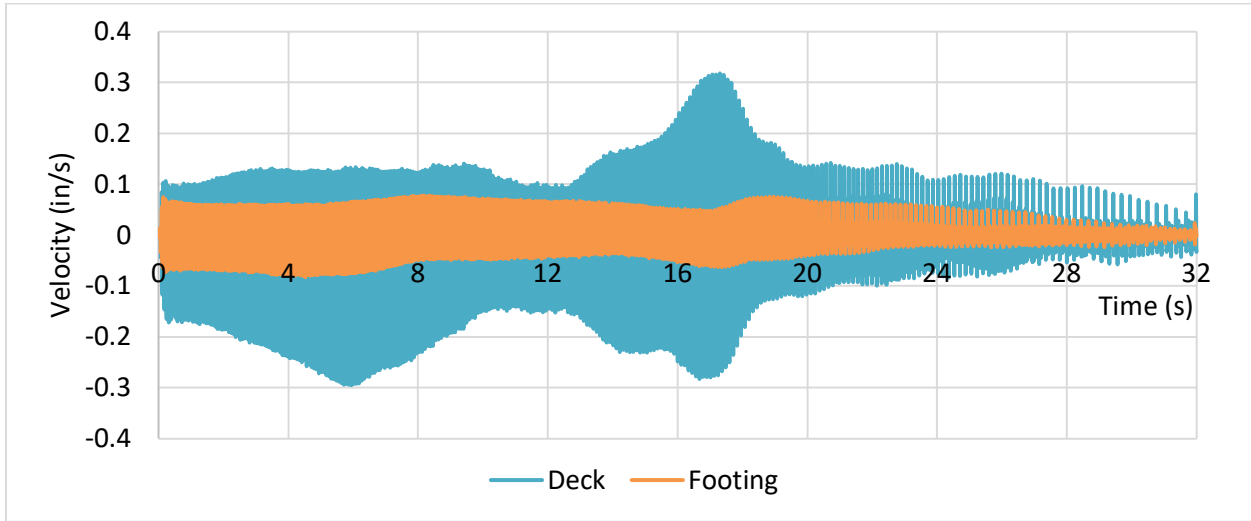
Fig. 19. Response of footing and deck to a 36 k chirp loading function (15-3 Hz)

Fig. 20 shows the power spectra at (a) the deck and (b) footing for the 80-10 Hz range, while Fig. 21 shows those for the 15-3 Hz range.
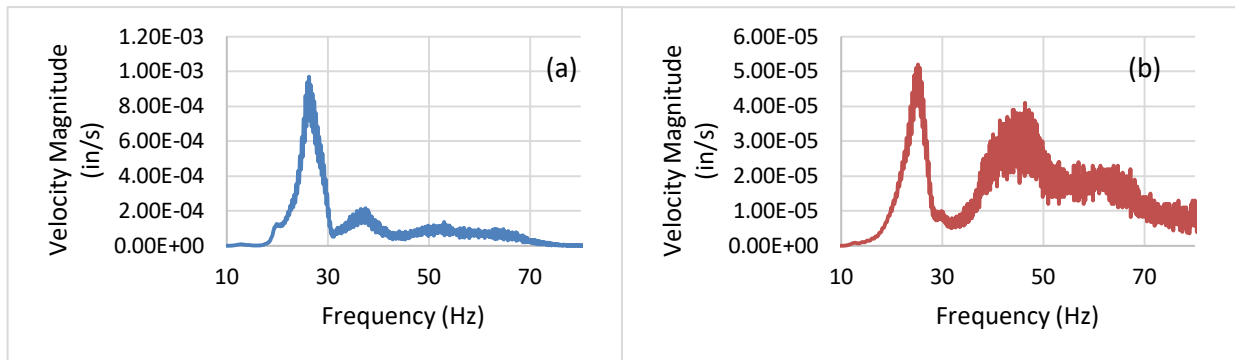
Fig. 20. Power spectra of response due to a chirp loading function 80-10 Hz at (a) deck and (b) footing.

19
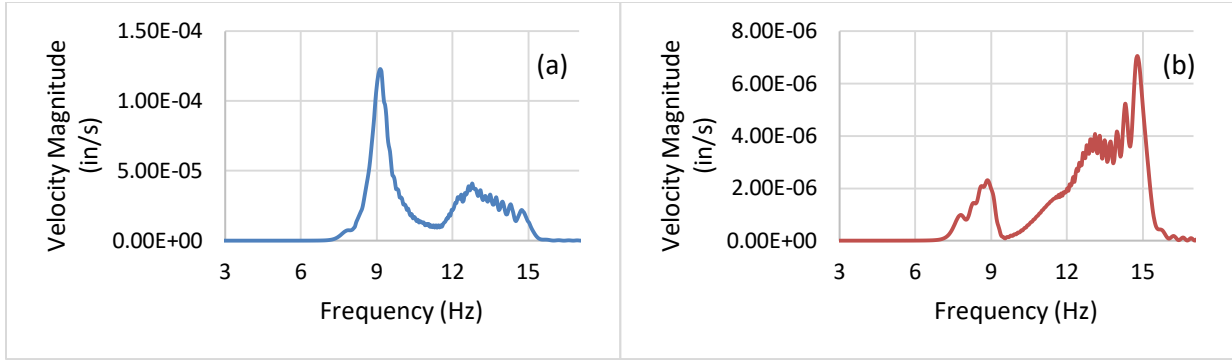
Fig. 21. Power spectra of response due to a chirp loading function 3-15 Hz at (a) deck and (b) footing.

From Fig. 20 and 21, the peaks in the plots represent resonances, or natural frequencies, of the soil/structure system. They are at 9.1 Hz, 14.8 Hz, and 26.2 Hz, respectively. However, the velocity magnitude around the 26.2 Hz resonance is the greatest. It is established that this frequency is the primary mode of vibration (or 3rd vertical mode). Hence, Table 2 shows the selected frequency to capture the response of the bridge around the primary resonance by approximating the system as a single degree of freedom (SDOF) system. This is crucial for establishing a site response analysis for displacement, velocity, and acceleration. In such a manner, the maximum response of each system will occur at different frequencies around the resonance. In the following set of tests, a steady-state shaking was carried out as defined in Table 2. The load magnitude for this set of tests was 24 k. Fig. 22 shows the steady-state response at the footing level of the bridge shaking at 26 Hz. This was the highest velocity response across all frequencies. Therefore, this record was used as a benchmark to validate the FEM model and confirm numerical results, as will be discussed in the next section.
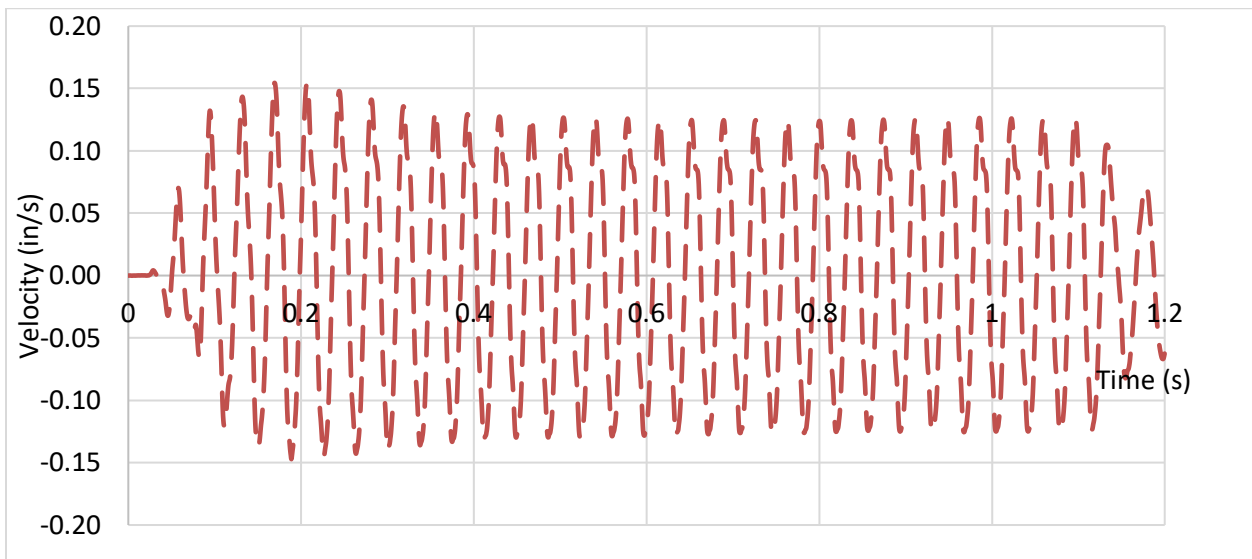
Fig. 22. Footing response to steady-state shaking at 26 Hz

Comparison of Field and FEM Model Results

The FE analysis and simulation of T-Rex loading was carried out in the time domain, the results of which were used to both validate the FEM models results and compare against the experimental results. Fig. 23 shows the T-Rex loading force, which was an input for the model. The force magnitude was 24 k. A deformed shape of the bridge response at one instant of time of bridge shaking is depicted in Fig. 24. It can be observed that it is possible to capture a notable response at the footing level by applying the load at the deck level.
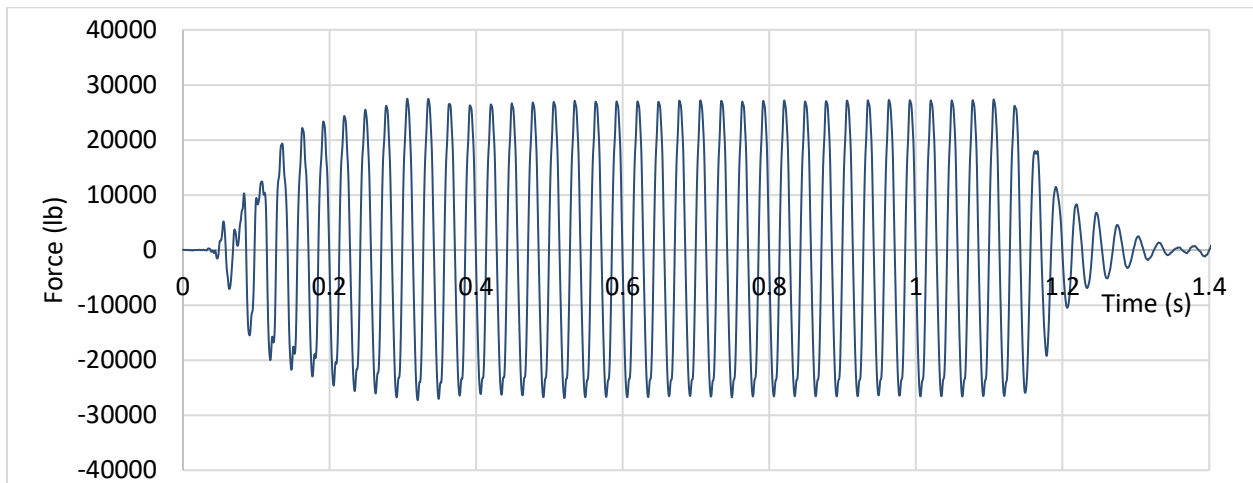
Fig. 23. Force input used in numerical model.
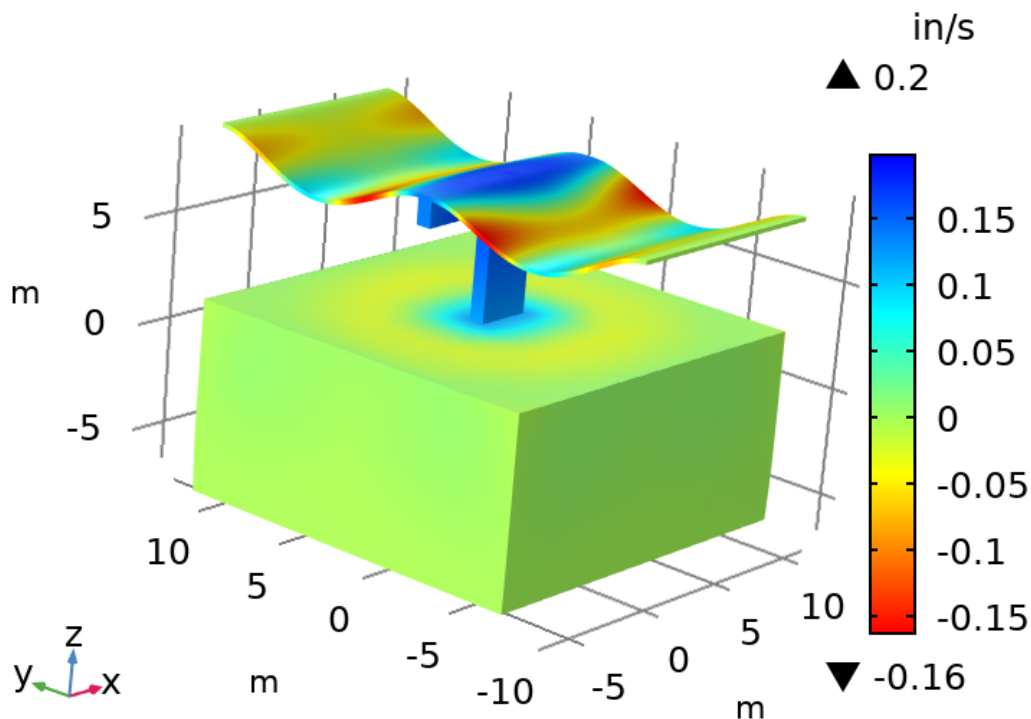
Fig. 24. Deformed shape of the bridge during one time instant of shaking.

For the purpose of this study, the response from the numerical simulation at the footing level and how it compares to the experimental results is of paramount importance. Fig. 25 shows a sample of this comparison. There is a good match between the numerical and experimental results across the entire time history. The model was built based on the parameters included in Table 3.
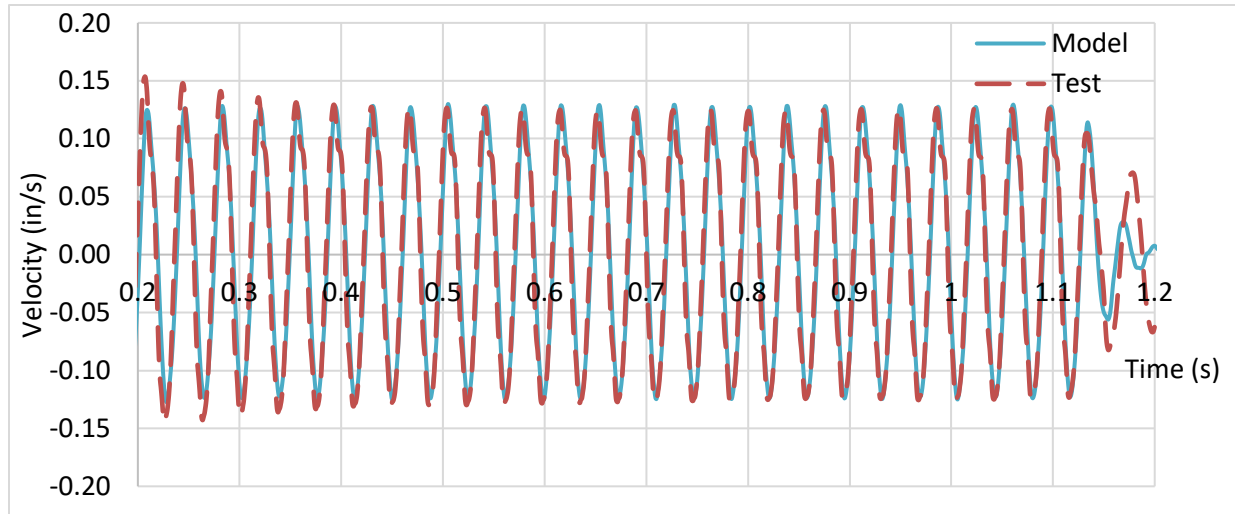
Fig. 25. Response of footing from numerical model and experimental test results due to steady-state loading.

Exploration of Parameters of an Unknown Foundation

After establishing that the numerical model was able to capture the response of this complex soil/structure dynamic response problem, it was utilized as a vehicle in identifying parameters of an unknown foundation. This was done by sweeping various geometric and material parameters to emulate the unknown foundation. Three main parameters (two geometric and one material) were included in the current study:

- Depth of the footing (distance from the ground surface to bottom surface of footing,
- Width of the footing (shorter dimension of footing), and
- Shear wave velocity of soil (an indicator of soil shear strength parameters).

Guidelines for the footing design/construction that are available in codes/standards were excluded from limiting the range of values of the parameters. For instance, there is a required minimum footing depth to avoid environmental effects and degradation. Additionally, there are recommended length-to-width ratios for sizing footings in design codes. Such criteria can be helpful in eliminating more variables for future studies. However, for the purpose of proving the concept of the study, only physical limitations are abided, albeit they are hypothetical. An example of this is the minimum footing dimensions considered. From a structural stability point of view, the minimum footing dimension used were those of the pile; any less than that would be unstable structurally. In essence, the only information present is what is visible from the bridge (the soil surface and the superstructure). Similarly, the minimum depth the footing can have is its own height (thickness). An assumption in the current study is that the bridge is supported by a shallow foundation and not by piles. Table 4 summarizes the range of values considered in the parametric sweeps carried out in the current study. Damping was also excluded since it can be determined from the response of the bridge/soil during shaking.

Table 4. Summary of Parameters Swept in Numerical Models for Footing Identification

Parameter	Range	Step	Units
D_f	F_h-3	0.5	m
F_w	P_w-6	1	m
V_s	100-450	50	m/s

Fig. 26 presents the effect of select footing depths indicated in Table 4, in comparison to the test results. It is qualitatively evident that setting the depth less than 2.5 m would lead to a much greater average error (~25%) when the width was set to 2.762 m. Setting the depth as 2.5 m provided the best fit of the experimental test results. Furthermore, Fig. 27 displays the effect of footing width (shorter dimension) on the response. The response of the footing was more sensitive to this parameter compared to the depth by looking at the same increment (1 m) when the depth was so to 2.5 m. It can be deduced that setting the width of the footing equal to the hypothetical pier width (0.762 m) or even a practical/possible width of (1.762 m) led to large errors in the response compared to the actual test results. Such can be >100% in the former and (80-90%) in the latter. The least error was when the footing width was set to 2.762 m. Although it is still not a perfect match, this dimension provided the best fit of the experimental data. An interesting behavior exhibited was increasing the footing width further did not lead to a better fit. This will be addressed in a continuation of the current study.

Figs. 28(a), (b), and (c) show the effect of having different materials or the shear wave velocity. The selected values for comparison were 200, 300, and 400 m/s. Such values emulate the transition from soft clays to medium and dense sands. The best match between the model and the experimental results was when the velocity was set to 400 m/s. While it is not a perfect match, the errors are lower than for 200 and 300 m/s cases. The errors in the case of 200 m/s ranged from 25% to 100%, 25% to 50% in the 300 m/s case, and from 2% to 25% in the 400 m/s case. It can be deduced that for the purpose of identification of unknown foundations, the footing response shows more sensitivity to geometric parameters, such as the footing depth and width, compared to material properties. This is especially true when the measurements are done in a linear range. This a promising finding since it shows that using large-amplitude mobile shakers, in tandem with well-defined 3D FEM models, a foundation can be identified in a nondestructive manner. On the other hand, having more accurate material properties (shear wave velocity in this case) can lead to a better estimation of the ultimate bearing capacity of the footing, which is also an important factor in the identification of unknown foundations. Lastly, when the footing width is set as 2.762 m, the footing depth as 2.5 m, and the shear wave velocity as 400 m/s, the match shown in Fig. 25 is achieved. This establishes these values as good approximations to the actual dimensions of the footing and soil shear wave velocity
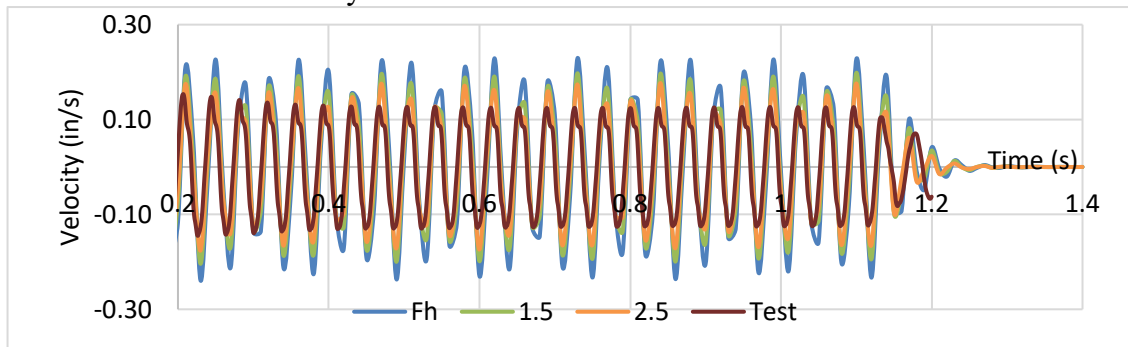
Fig. 26. Effect of footing depth on footing response (depths in m)
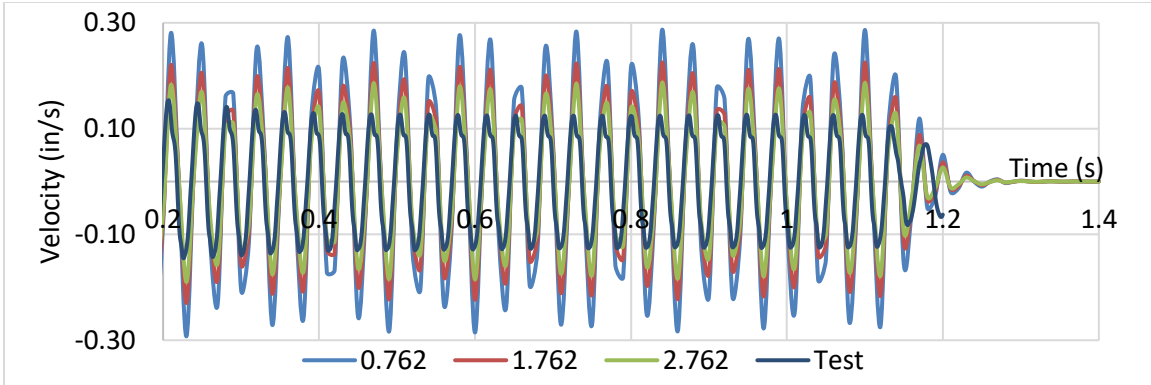
Fig. 27. Effect of footing width on footing response (widths in m)
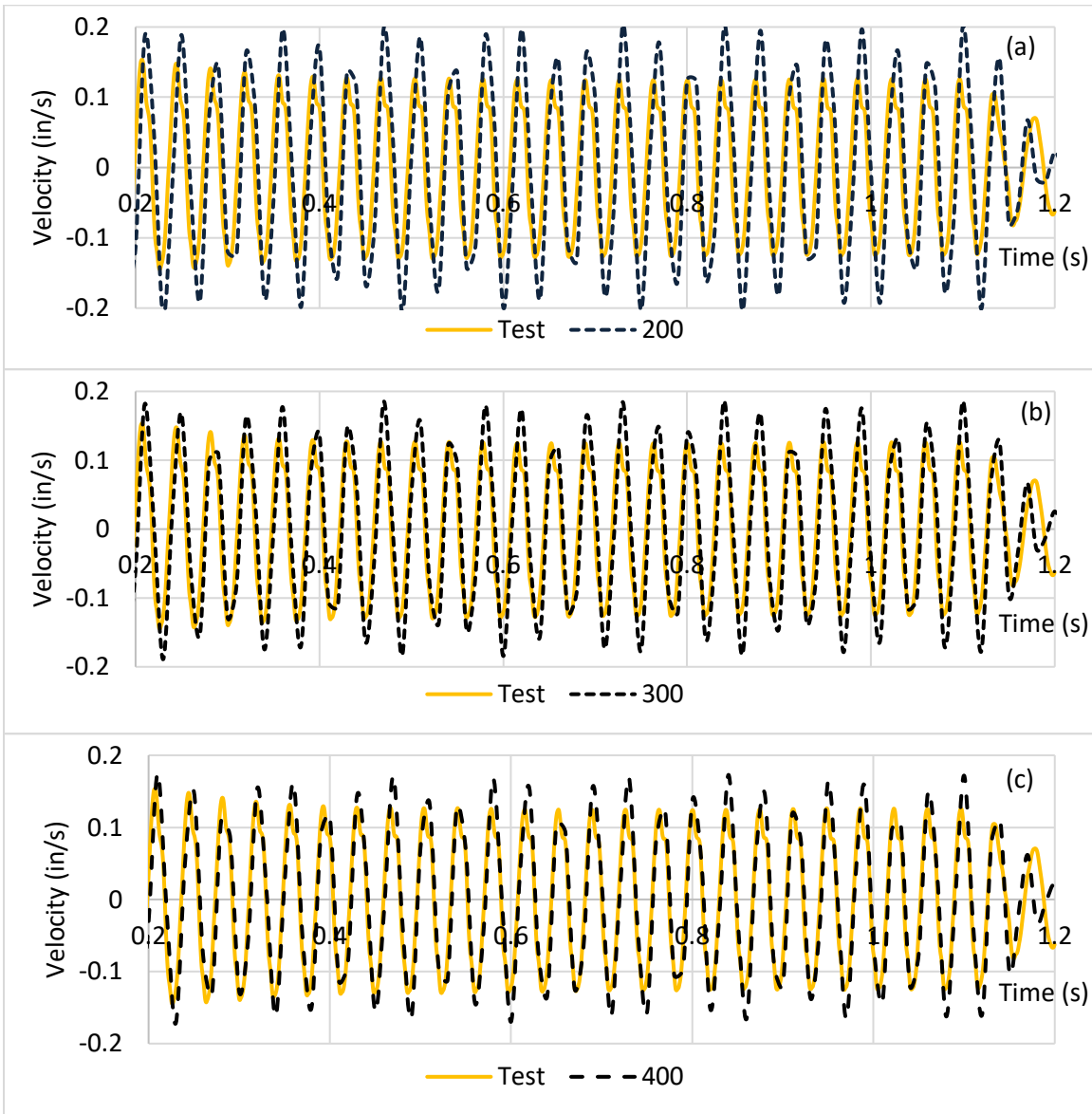
Fig. 28. Effect of changing V$_s$ on footing response; (a) V$_s$ = 200 m/s, (a) V$_s$ = 300 m/s, and (c) V$_s$ = 400 m/s.

Estimation of Soil Properties and Ultimate Bearing Capacity

The response of the bridge to dynamic shaking was used to evaluate the shear modulus of the supporting soil. This is done in a scenario where the geometry of the footing is known either by matching the actual response to a FEM model as presented earlier or by estimating dimensions of the footing from knowledge of the superstructure. To entertain the novelty of this method, the latter procedure is adopted for this example. The determination of shear modulus of the supporting soil, the footing is assumed to be a massless prism on an elastic homogenous half-space. This allows for the exploitation of dynamic soil-structure interaction to determine soil properties and how they change with frequency. Since the objective is to find the low-strain shear modulus, stiffness (load divided by displacement) of the footing is obtained from the steady-state response to shaking at the low-frequency range. The steady-state displacements were obtained by integration of the velocity records in the time domain for all tested frequencies using Simpson's Rule. Fig. 29 shows a sample displacement record obtained by integration, with a steady-state response of ~0.0012 in [0.03 mm]. The steady-state force and displacement were determined for the tested frequency range, as illustrated in Fig. 30 (a) and (b), respectively. The total vertical impedance is defined as:

$$S_v = F_v(t)/U_v(t) \tag{6}$$

where $F_v(t)$ and $U_v(t)$ are the harmonic vertical force and displacement respectively.
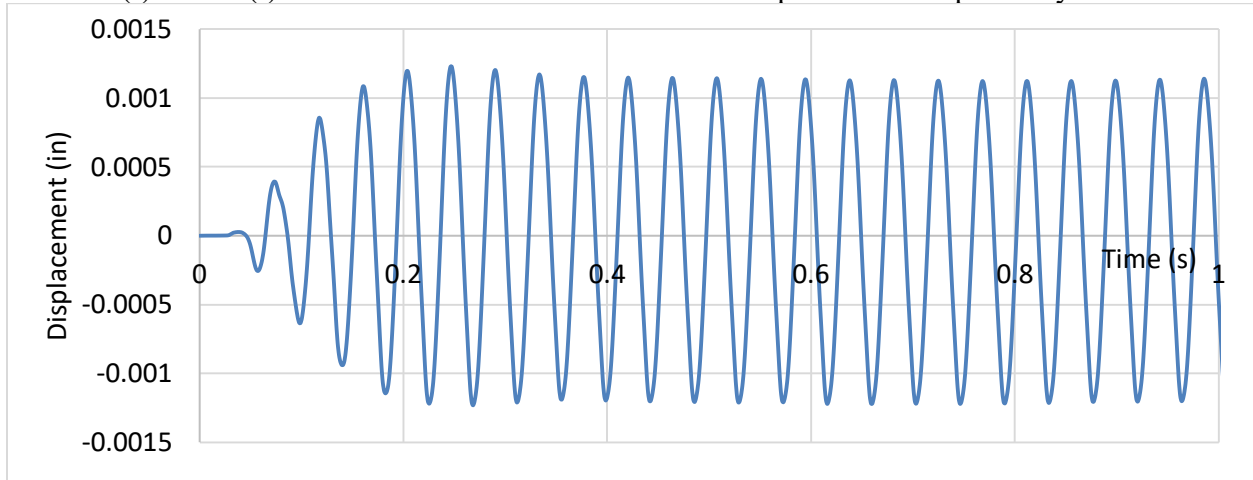
Fig. 29. Steady-state displacement obtained by integration of velocity @23 Hz

Total impedance includes a stiffness component and a damping component as a function of frequency. Therefore, impedance can be expressed as

$$S_v(\omega) = K(\omega) + i\omega C(\omega) \tag{7}$$

where $K(\omega)$ is the dynamic stiffness and $C(\omega)$ is the sum of material and radiation damping. The complex notation is because F_v is typically out of phase with U_z (Gazetas, 1991; Pais & Kausel, 1988). The damping term is essentially negligible at lower frequency ranges, which means that total impedance is solely comprised of the stiffness term. This enables the estimation of stiffness directly from the impedance function. Impedance as function frequency is shown in Fig. 31. It can be observed that the impedance is almost constant, about 60,000 k/in, up to a frequency of 15 Hz. This indicates that is the portion of the graph is still within static stiffness. This obtained stiffness includes the effect of footing embedment since it is obtained experimentally, which has to be taken into account while estimating shear modulus.
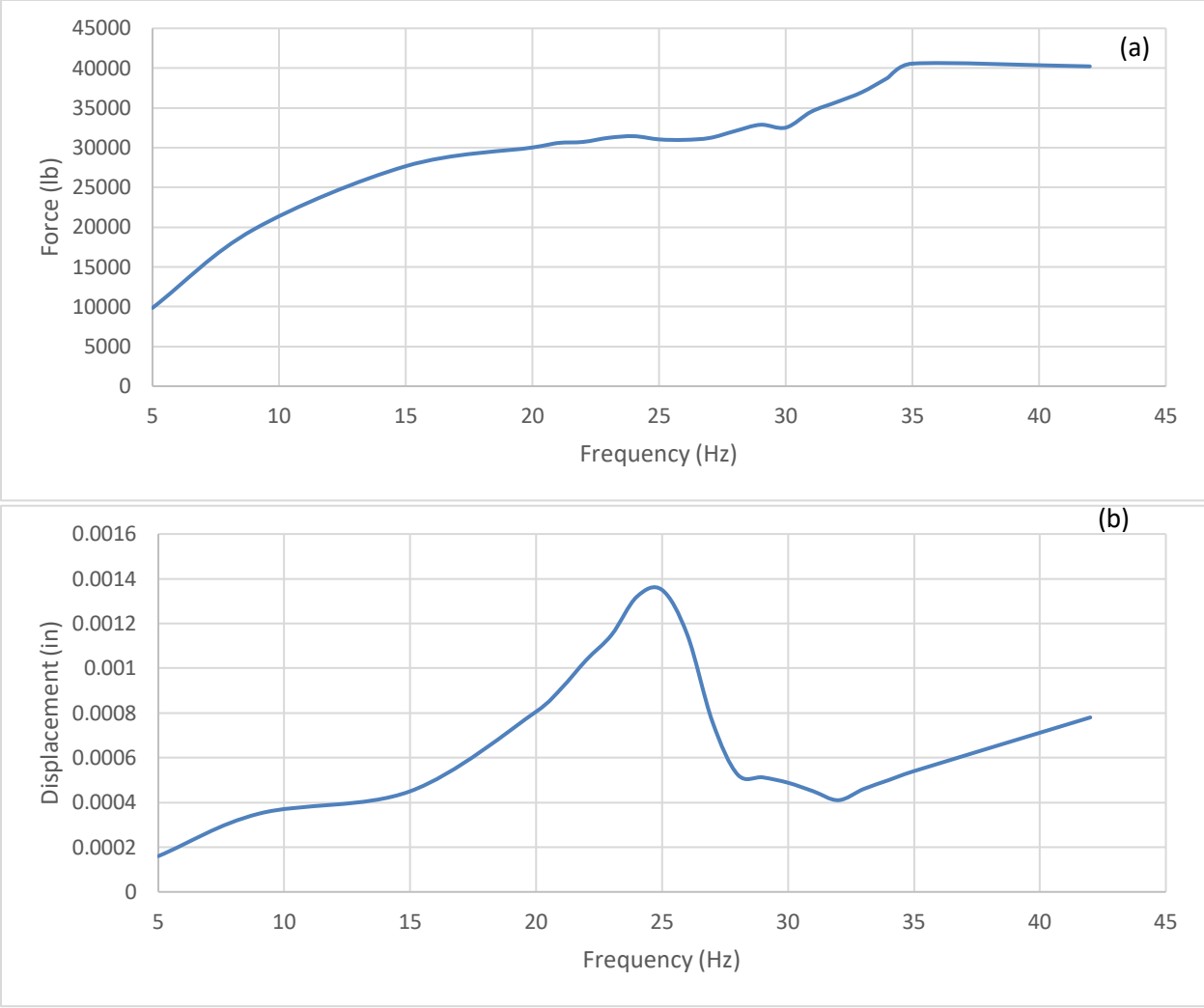
Fig. 30. Steady-state (a) force and (b) displacement at the geophone near footing due to T-Rex shaking
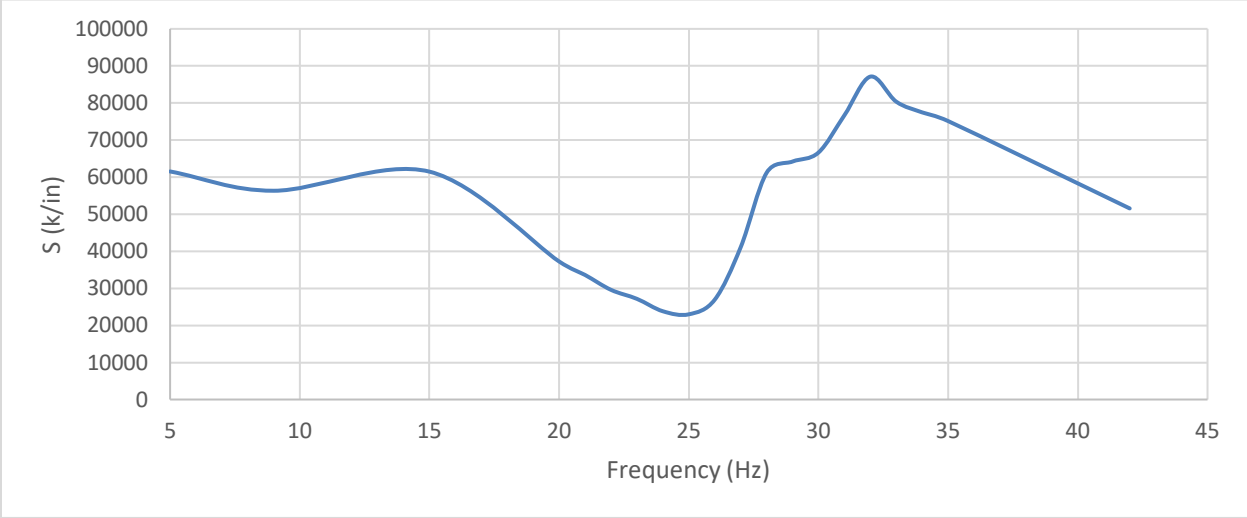
Fig. 31. Experimental impedance curve resulting from dynamic testing

A widely-accepted expression for a fully embedded rectangular footing is:

$$K_{emb} = \frac{2LG}{1-\upsilon} \, S_z \left[1 + \frac{D}{21B}\left(1 + \frac{A_b}{3L^2}\right)\right]\left[1 + 0.19\left(\frac{A_w}{A_b}\right)^{\frac{2}{3}}\right] \quad (8)$$

where L and B are half-length and half-width of footing, G is the shear modulus, D is the embedment depth (from the ground surface to bottom surface of footing), υ is Poisson's ratio, A_b is the bearing area = 2L x 2B, A_w is the sidewall contact area = 2(2L+2B)d, where d is the thickness of the footing, and S_z is a vertical stiffness parameter for an equivalent circular foundation approximation = $0.73 + 1.54 (A_b/4L^2)^{0.75}$. Clearly, the shear modulus of soil can be approximated if appropriate values for footing geometry are plugged in equation (8); K_{emb} is ~60,000 k/in, and υ is 0.33 for sand. Since the tested bridge is supported by hammerhead piers with a length of 36', a reasonable approximation of footing length is 50% of that width. A footing aspect ratio (L/B) can be used to define the width of the footing. Furthermore, a typical embedment ratio (D/B) range from 1-2 was used. Lastly, the thickness of the footing was estimated to be 6 ft, which is deemed sufficient to resist dead and live loads. Table 5 summarizes the results of shear modulus estimation for this scenario, in addition to using actual footing dimensions. The obtained modulus for both scenarios is regarded relatively high. However, the values obtained for shear modulus are in reasonable agreement with the shear wave velocity profile shown in Fig. 15. In addition, it is idealized that load resistance/bearing is attributed to the soil properties at the soil-footing interface. Nevertheless, there is a contribution from deeper soil elements that have even higher shear modulus or strength parameters. This leads to such an apparent increase in shear modulus. On the other hand, using the estimated dimension led to a fair estimation of the shear modulus. This means that as long as the dynamic force and response are measured accurately, the dimension of the footing can be iterated to reach the best match with the shear wave velocity profile using the impedance function obtained from testing. This is a promising finding since it promotes the use of large-amplitude mobile shakers as nondestructive method for exploring unknown foundations. Furthermore, once the geometry has been confirmed, the ultimate bearing capacity can be evaluated as aforementioned.

Table 5. Estimation of Shear Modulus Using Experimental Results with Two Sets of Footing Geometry

Scenario	2L (ft)	2B (ft)	L/B (ft)	D (ft)	d (ft)	G (ksf)[MPa]
Estimated Geometry	18	9	2	9	6	12,000[574]
Actual Geometry	15	9	1.67	8	5	10,830[518]

For the estimation of ultimate bearing capacity, classical methods based on empirical formulations require the knowledge of the geometry of the footing and soil material properties. The geometric aspects include the footing dimensions, ground slope, and depth. As for material properties, shear strength parameters (angle of internal friction and/or cohesion) are required, in addition to the unit weight of soil. In addition, the groundwater table position is essential in determining the overburden pressure and appropriate unit weight to be used in the bearing capacity estimate. Moreover, load inclination and loading eccentricity can also affect the ultimate bearing capacity of a footing.

The only measured soil parameter that can be correlated to the shear strength in the current study was the shear wave velocity. The shear wave velocity of sand is inherently related to its shear strength parameters, although it is measured at a small strain. This is due to the dependence of the angle of internal friction on the void ratio and confining pressure. There is an inverse relationship between the void ratio and shear wave velocity, and the friction angle. Therefore, the

knowledge of either one can be a good indicator of shear strength. Another advantage of using the shear wave velocity as an indicator of shear strength parameters in sands is that there is no to very low effect of moisture on the shear wave velocity (Dong & Lu, 2016). Hence, a changing position of the ground water table will have minimal effects on the value of shear wave velocity. Nevertheless, it would greatly affect the effective stresses, which have to be accounted for in the calculation of ultimate bearing capacity.

For the purpose of estimating ultimate bearing capacity, the angle of internal friction (ϕ) was estimated as 36° from several reported correlations of SPT value and V_s (Kumar, Bhargava, & Choudhury, 2016; Wair, DeJong, & Shantz, 2012). Cohesion was set as 0 since it is a sandy site. As for the ground water table, a conservative approach was used in this study, and the footing was considered to be submerged, although the measurements were conducted in the dry season. This is the case because the bridge is an overpass over a channel, which may submerge the footing in the wet season. Another practical assumption undertaken was that any moment acting on the footing is negligible compared to the axial load; load distribution is uniform on the bottom of the footing. In addition, the load was considered to be acting perfectly axial and concentric from the pier onto the footing. Using Vesic's method (Vesić, 1973), the ultimate bearing capacity of the tested footing is estimated to be 42 ksf (2,050 kPa), or can support a load of 5,610k (25,400 kN).

CONCLUSIONS

In this project, the use of large-amplitude shakers to explore unknown foundations and evaluate ultimate bearing capacity is presented. T-Rex, a shaker from NHERI, was deployed to impose controlled forced vibration on an actual bridge in Oregon. Several test runs at varying load magnitudes and forcing functions were carried in the experimental program. Multiple geophones were utilized to capture the response to vertical shaking. In addition, a 3D FEM model of the bridge was developed to numerically simulate the response to shaking. A parametric study was carried out to evaluate the effect of material and geometric properties on the response. The model was validated by the experimental results. Furthermore, the soil shear wave profile was determined experimentally to confirm some of the results obtained in the analysis and as a benchmark for the FEM model. The following can be concluded from the current study:

- A shear wave velocity profile was determined for the soil at the tested bridge site. The shear wave velocity at the level of the footing was about 450 m/s.
- Chirp functions for vertical loading were utilized to identify natural frequencies of the soil-structure system. Three resonant frequencies were determined at 9.1 Hz, 14.8 Hz, and 26.2 Hz. The dominant eigenfrequency was 26.2 Hz since it resulted in the highest response under the same driving load magnitude.
- A parametric study was conducted using a validated FEM model to assess the effects of material and geometry parameters of the footing on the response. This was done as part of an exploration of unknown foundations. The parameters included were footing depth, width, and soil shear velocity. Footing response shows more sensitivity to geometric parameters such as footing depth and width compared to material properties when matching with the actual response.
- Determining the soil shear modulus was carried out for a scenario of estimated footing dimensions based on the superstructure and was compared to the actual geometry. Both

cases yielded shear wave velocity fairly comparable to that obtained from the shear wave velocity profile.

- The ultimate bearing capacity of the tested footing is estimated to be 42 ksf (2,050 kPa), or can support a load of 5,610 k (25,400 kN) based on both the shear wave velocity profile obtained from SASW testing.
- Large-amplitude mobile shakers can be used for the purpose of foundation exploration if the steady-state force and response of footing - hence impedance functions - are accurately measured. This was done for the soil/bridge system tested in the current study

REFERENCES

Agrawal, A. K., Jalinoos, F., Davis, N., Hoomaan, E., & Sanayei, M. (2018). *Foundation Reuse for Highway Bridges* Retrieved from

Dong, Y., & Lu, N. (2016). Dependencies of Shear Wave Velocity and Shear Modulus of Soil on Saturation. *Journal of Engineering Mechanics, 142*(11), 04016083. doi:10.1061/(ASCE)EM.1943-7889.0001147

Gazetas, G. (1991). Formulas and Charts for Impedances of Surface and Embedded Foundations. *Journal of Geotechnical Engineering, 117*(9), 1363-1381. doi:doi:10.1061/(ASCE)0733-9410(1991)117:9(1363)

Gucunski, N., & Woods, R. D. (1992). Numerical simulation of the SASW test. *Soil Dynamics and Earthquake Engineering, 11*(4), 213-227. doi:https://doi.org/10.1016/0267-7261(92)90036-D

Kumar, R., Bhargava, K., & Choudhury, D. (2016). Estimation of Engineering Properties of Soils from Field SPT Using Random Number Generation. *INAE Letters, 1*(3), 77-84. doi:10.1007/s41403-016-0012-6

Menq, F.-Y., Stokoe, K. H., Park, K. I., <st1:personname w:st="on">Rosenblad, B., & Cox, B. R. (2008). *Performance of Mobile Hydraulic Shakers at NEES@UTexas for Earthquake Studies*. Paper presented at the *14th World Conference on Earthquake Engineering*, <st1:place w:st="on"><st1:city w:st="on"> Beijing , <st1:country-region w:st="on">China</st1:country-region>.

Nazarian, S., Stokoe, K. H. I., & Hudson, W. R. (1983). *Use of spectral analysis of surface waves method for determination of moduli and thicknesses of pavement systems*. Paper presented at the Transportation Research Board, Washington, D.C.

Olson, L. (2005). *Dynamic Bridge Substructure Evaluation and Monitoring.* Retrieved from

Olson, L., Jalinoos, F., & Aouad, M. (1998). *Determination of Unknown Subsurface Bridge Foundations*. Retrieved from

Pais, A., & Kausel, E. (1988). Approximate formulas for dynamic stiffnesses of rigid foundations. *Soil Dynamics and Earthquake Engineering, 7*(4), 213-227. doi:https://doi.org/10.1016/S0267-7261(88)80005-8

Stokoe, K., Cox, B., Clayton, P., & Menq, F. (2017). *NHERI@UTexas Experimental Facility: Large-Scale Mobile Shakers for Natural-Hazards Field Studies*. Paper presented at the *16th World Conference on Earthquake Engineering*, Santiago, Chile.

Vesić, A. S. (1973). Analysis of ultimate loads of shallow foundations. *Journal of the Soil Mechanics and Foundations Division, 99*, 45-73.

Wair, B. R., DeJong, J. T., & Shantz, T. (2012). Guidelines for Estimation of Shear Wave Velocity Profile. In *PEER Report 2012/08*: Pacific Earthquake Engineering Research Center.